nature geoscience

ARTICLES

https://doi.org/10.1038/s41561-019-0440-5

The susceptibility of Oklahoma's basement to seismic reactivation

F. Kolawole[1], C. S. Johnston[1], C. B. Morgan[1,4], J. C. Chang[2], K. J. Marfurt[1], D. A. Lockner[3], Z. Reches[1] and B. M. Carpenter[1*]

Recent widespread seismicity in Oklahoma is attributed to the reactivation of pre-existing, critically stressed and seismically unstable faults due to decades of wastewater injection. However, the structure and properties of the reactivated faults remain concealed by the sedimentary cover. Here, we explore the major ingredients needed to induce earthquakes in Oklahoma by characterizing basement faults in the field, in seismic surveys and via rock-mechanics experiments. Outcrop and satellite mapping reveal widespread fault and fracture systems with trends that display a marked similarity to the trends of recent earthquake lineaments. Our three-dimensional seismic analyses show steeply dipping basement-rooted faults that penetrate the overlying sedimentary sequences, representing pathways for wastewater migration. Experimental stability analysis indicates that Oklahoma's basement rocks become seismically unstable at conditions relevant to the dominant hypocentral depths of the recent earthquakes. These analyses demonstrate that the geometry, structure and mechanical stability of Oklahoma's basement make it critically susceptible to seismic reactivation.

The dramatic increase in widespread seismicity in Oklahoma since 2009 (Fig. 1a), which has been attributed to large-scale wastewater injection, exceeded the seismicity level of other areas of wastewater injection in Central and Eastern United States and Canada[1–4]. Most Oklahoma earthquakes have occurred on previously unknown fault segments within the Precambrian crystalline basement[2], yet the nature of basement structure is largely unknown. For example, the largest earthquake in Oklahoma, the 2016 moment magnitude (M_w) 5.8 Pawnee event (Fig. 1a), ruptured an unmapped fault trending west-northwest–east-southeast (now called the Sooner Lake Fault). Similarly, the 2016 M_w 5.1 Fairview earthquake (Fig. 1a) ruptured a previously unmapped segment of the Galena Township Fault[5,6].

Wastewater injection can induce earthquakes along pre-existing faults via various triggering mechanisms, including direct increase of pore pressure within fault zones[7] and poroelastic stress transfer from injection sites to remote faults[6]. While these mechanisms may induce fault slip, the induced fault slip may occur either as stable creep or as unstable rupture, and the seismic stability of a fault zone depends strongly on its composition and the loading conditions. Although much is known about the stability of faults in common crystalline rocks[8], the seismic stability of the granite–rhyolite provinces of the US midcontinent, which have undergone multiple phases of tectonic deformation and hydrothermal alteration[9–12], are not known. Further, the fact that significant wastewater injection in some parts of Oklahoma has induced only limited seismicity[3] raises questions on (1) the hydraulic connectivity between injection zones and the basement and (2) the rheology and stress state of the basement.

Oklahoma basement rocks form part of a Precambrian igneous province that extends across the US midcontinent[9] (Fig. 1c). Thus, we envision that a better understanding of induced seismicity in Oklahoma and better knowledge of the nature of its basement faults can lead to injection strategies that mitigate the likelihood of harmful induced or triggered earthquakes. Such mitigating strategies can be applied to areas underlain by a similar basement to Oklahoma in the Central United States and other parts of the world with active wastewater injection operations[1].

Here, we address deficiencies in understanding the controlling mechanisms of the widespread induced seismicity in Oklahoma. We characterize the patterns of fault and fracture systems in the Precambrian basement exposures of southern Oklahoma and the structure of subsurface basement faults in the region of earthquake activity and experimentally determine the seismic stability of the basement rocks at in situ conditions. These analyses provide the first documented link between basement structure and the current earthquakes, show potential pathways between wastewater injection intervals and the deeper Precambrian basement and explain the depth distribution of the earthquake hypocentres.

Oklahoma basement

The Oklahoma basement is in the southern part of the 1.35–1.48 Ga granite–rhyolite provinces of the US midcontinent[9], which extend from west Texas to western Ohio[9] (Fig. 1c). These provinces are dominated by siliceous igneous rocks of granites and rhyolites and their metamorphic derivatives[9,13]. The Southern Granite–Rhyolite Province (1.35–1.40 Ga) has undergone multiple phases of tectonic deformation that included Precambrian north-northeast/south-southwest rifting followed by reverse faulting[14], Early to Middle Cambrian northwest–southeast rifting and the related Southern Oklahoma Aulacogen[15]. While the Late Palaeozoic tectonic phases are best documented in the sedimentary sequence[15–17], they certainly affected the underlying crystalline basement.

Most of the recent earthquake activity in Oklahoma has occurred in the north-central region of the state (Fig. 1a) where the crystalline Precambrian basement is covered by a 1- to 3-km-thick veneer of sedimentary strata[13]. Due to this cover, our field analysis

[1]School of Geosciences, University of Oklahoma, Norman, OK, USA. [2]Hawaiian Volcano Observatory, United States Geological Survey, Hawaii National Park, HI, USA. [3]United States Geological Survey, Menlo Park, CA, USA. [4]Present address: Chesapeake Energy Corporation, Oklahoma City, OK, USA. *e-mail: brett.carpenter@ou.edu

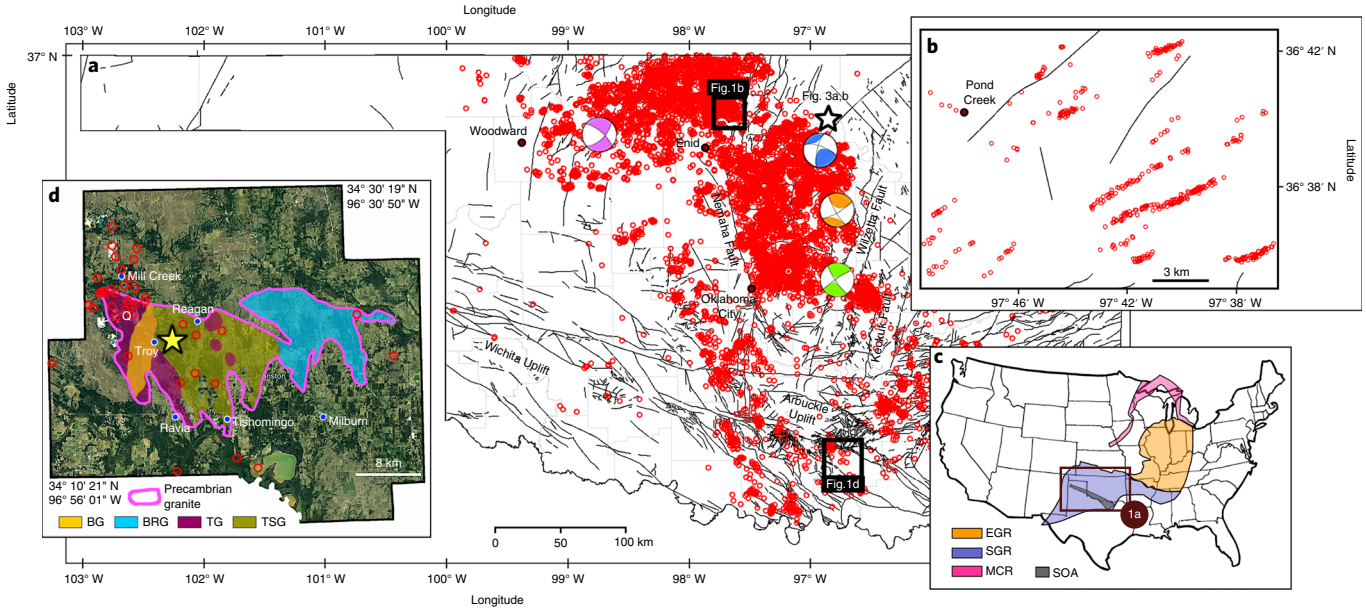

Fig. 1 | Earthquakes and basement lithology in Oklahoma. a, Earthquakes in Oklahoma for 2010–2017; red circles represent earthquake epicentres (Oklahoma Geological Survey catalogue; http://www.ou.edu/ogs/research/earthquakes/catalogs); thin black lines represent mapped faults[41]; focal mechanism solutions of $M_w > 5.0$ events represent 2011 M_w 5.7 Prague (green), 2016 M_w 5.1 Fairview (purple), 2016 M_w 5.8 Pawnee (blue), and 2016 M_w 5.0 Cushing (orange); black squares and white star indicate locations of stated figures. **b**, Close-up of region marked 'Fig. 1b' in **a** showing a discrepancy between lineaments of relocated earthquakes (red circles) and previously mapped faults. **c**, Precambrian Terranes in the US midcontinent[9]; EGR, Eastern Granite–Rhyolite Province; SGR, Southern Granite–Rhyolite Province; MCR, Midcontinent Rift; SOA, Southern Oklahoma Aulacogen (Cambrian). Panel reproduced from ref. [9], Elsevier. **d**, Close-up satellite image of region marked 'Fig. 1d' in **a** showing Precambrian basement exposures[10], Johnston County, southern Oklahoma; Q, Martin Marietta Quarry; BG, Burch Granodiorite; BRG, Blue River Gneiss; TG, Troy Granite; TSG, Tishomingo Granite. Map data: Google, Landsat/Copernicus.

of basement structure focuses on the only major basement outcrop in Oklahoma, which is a >300 km^2 region in Johnston County (Fig. 1d). The exposed basement is composed of granites, granodiorites and gneisses, 1.36–1.39 Ga in age, that are locally intruded by subvertical diabase dykes of Precambrian and Cambrian ages[10,18]. Common hydrothermal alterations include calcite and epidote veins[10]. The northwest–southeast predominant trend of these dykes was influenced by pre-existing structural imprints of previous tectonic phases[10,18]. Since the basement of Oklahoma has a similar thermo-tectonic history to that of the other areas underlain by the Precambrian granite–rhyolite provinces[9], we envision that a better understanding of the structure of the Oklahoma basement would provide some insight into the dynamics of induced seismicity in the other areas.

Exposed fault and fracture systems

In our fieldwork, we characterize the fault and fracture systems in basement outcrops of the Tishomingo, Troy and Blue River granites (Fig. 1d). The exposures display multiple networks of subvertical fractures that locally control the hummocky surface morphology and stream directions (Fig. 2a and Supplementary Fig. 1a,b). Most of the fractures show tensile features, including rough surfaces, en echelon segmentation and rare mineralization (Supplementary Figs. 1a and 2a,b). These tensile indicators are common in coarse-grained granites[19,20], and the grain size of the studied granites ranges from 1 to 3 cm. The examination of hundreds of fractures revealed only a small number of strike-slip faults with minor displacements of 2–36 cm and sporadic occurrences of slickenlines (Supplementary Fig. 2a,b).

While most fractures are widely spaced, we found several discrete zones of intense damage with multiple closely spaced fractures (for example, Fig. 2a and Supplementary Fig. 1b) exhibiting the following features: (1) a predominant fracture set with a cross-cutting minor set that together form rhombohedral blocks (Fig. 2b), (2) systematic increase of fracture density towards the core of the zone (Fig. 2a,b), (3) multiscale, dense pattern of anastomosing fractures with local gouge (pulverized zone) (Fig. 2b,c) and (4) partial control of the local drainage system (Fig. 2a and Supplementary Fig. 1b). We interpret these damage zones as the upper portions of deeper immature strike-slip fault zones. The interpretation is based on documented observations and analyses of fault zones in crystalline rocks that revealed similar features of subparallel arrays of steeply dipping fractures with small (centimetre scale) strike-slip displacements[21]. Both field and subsurface observations have also shown that the intensity of fracturing and damage is highest at the fault core and decreases with distance from the fault zone[22,23]. This pattern is similar to the present observation.

A striking feature of the fractures in the granite exposures is the consistent trends of both tensile fractures and small faults with predominant trends of northwest–southeast (317° ± 6.4°) and northeast–southwest (241° ± 2°) and a minor approximately north–south trend (Fig. 2d and Supplementary Figs. 1 and 2a,b). These trends also fit the northwest–southeast and northeast–southwest trends of the regional pegmatite and diabase intrusions[18] (Supplementary Fig. 2c). We extended the scale of the field analyses by mapping fracture systems on satellite images of the granite exposures (Supplementary Fig. 1b). The mapped 745 fracture segments, which range from 3 to 200 m in length with a cumulative length of 17.3 km, reveal two dominant sets of northwest–southeast (308° ± 3.6°) and northeast–southwest (234° ± 3.7°) (Supplementary Fig. 1c). In summary, the exposed Precambrian basement displays a multiscale consistency of the fault and fracture systems that generate a tectonic grain of two prominent trends (Fig. 2d and Supplementary Fig. 1c). Geochronological and structural analyses of the igneous

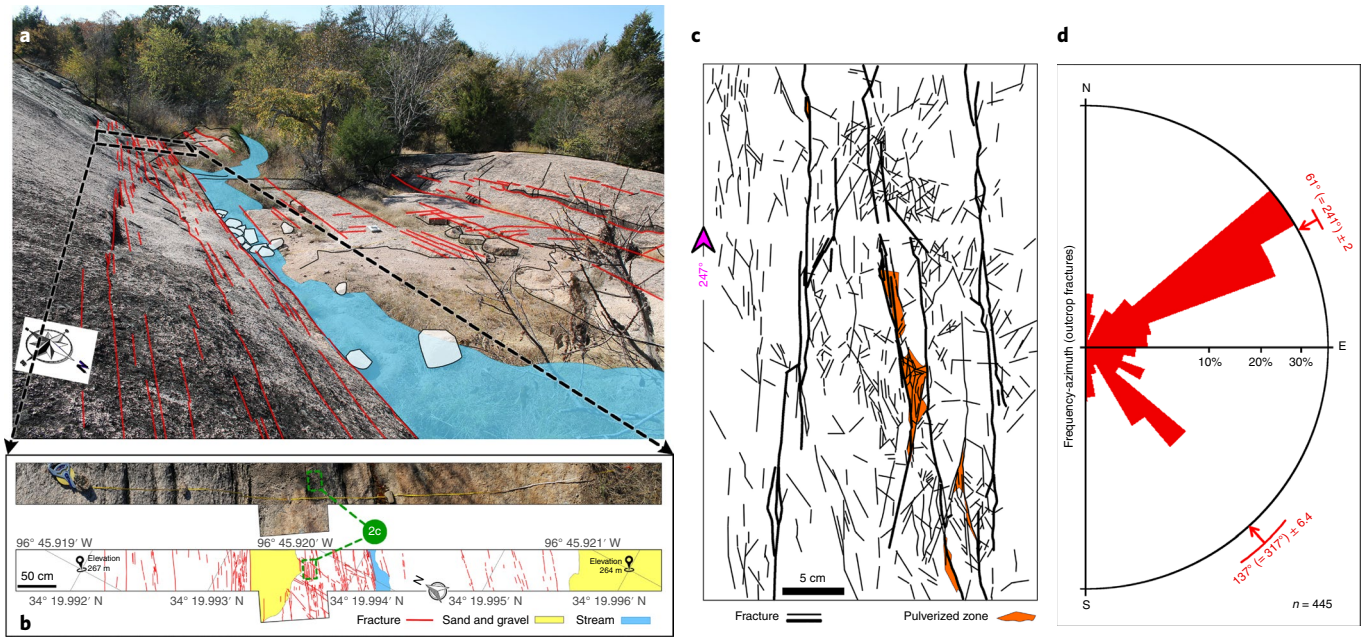

Fig. 2 | Outcrop fractures. a, Precambrian basement outcrop with a 241° trending zone of fracture clusters, interpreted as the upper portions of a deeper immature strike-slip fault zone (location: yellow star in Fig. 1d). **b**, Close-up photograph of the zone of fracture clusters with structural mapping. **c**, Close-up view with dense fracture network and gouge at the core of a fracture cluster (dashed green boxes and line in **b**). **d**, Frequency-azimuth distribution of 445 fracture segments from Fig. 1d. Structural trends are described as 'mean trend (= mean trend + 180°) ± s.d.'.

intrusions that used these prominent fracture trends indicate that the fractures are Precambrian in age[10,18].

Earthquakes and subsurface fault structures

As mentioned, the recent earthquakes have occurred in north-central Oklahoma (Fig. 1a) where the crystalline basement is covered by 1–3 km of sedimentary strata[13]. We examined the seismicity pattern via the relocation of 10,879 earthquakes of $M_w \geq 0$ covering the period 2010–2017 (Methods). The relocated epicentres display spatial clusters that form 717 distinct lineaments (for example, Fig. 1b) with two prominent trends of northwest–southeast (297° ± 3.6°) and northeast–southwest (239° ± 2.9°) (Supplementary Fig. 3a). These lineaments are reasonably interpreted as traces of reactivated faults[24]. We further examined the focal-plane solutions of 6,253 earthquakes of $M_w \geq 3$ for the period 2010–2018 (source: Oklahoma Geological Survey). These solutions revealed two dominant trends of seismic slip planes (307° ± 1.6° and 226° ± 1.6°) (Supplementary Fig. 3b) that are consistent with the trends of the epicentre lineaments (Supplementary Fig. 3a).

To determine the subsurface basement structure in the seismically active area, we used three-dimensional (3D) seismic reflection data (Methods) that cover a 114 km^2 area in Osage County, northern Oklahoma, located ~18 km from the 2016 M_w 5.8 Pawnee earthquake epicentre (Fig. 1a). The analysis reveals 16 subvertical fault zones, some of which (black arrows in Fig. 3a,b) cut through the upper basement, disrupting intra-basement reflectors, into the top of the Arbuckle group. These intra-basement reflectors, which are most likely related to mafic igneous sheet intrusions, have been observed in other parts of north-central Oklahoma[25]. Some of the mapped faults branch out into strands that offset the sedimentary formations above the Arbuckle group (Fig. 3a–c) and exhibit a 230- to 500-m-wide zone of splays (Fig. 3c) that depict the typical 'flower structures' of strike-slip faults. These basement faults range in length from 1.5 km to 7 km with variable trends (Fig. 3a,b and Supplementary Table 1), and their implications for Oklahoma's earthquakes are discussed in the section 'Oklahoma's susceptibility to seismic reactivation'.

Seismic stability of basement material

As noted, fluid injection can induce fault slip, but this slip may be manifested by either stable creep or seismic events[7,26], depending on the fault's seismic (that is, frictional) stability at the given temperature/pressure conditions[8]. We experimentally[27] analysed the frictional stability of basement rocks using four samples of cores from north-central Oklahoma and one outcrop sample from south-central Oklahoma (Methods, Supplementary Fig. 4a–c and Supplementary Table 2). These samples are representative of common crystalline rocks such as one might find anywhere in the exposed shield[10–12], where multiple phases of deformation are ubiquitous[9]. The experiments were performed at conditions relevant for the dominant seismicity depth range of 1.5–9.0 km. For the in situ conditions of both temperature and confining pressure, we used a geothermal gradient of 23 °C km^{-1} (ref. [28]) and a pore–fluid pressure gradient of 10 MPa km^{-1} to produce an effective confining pressure gradient of 17.5 MPa km^{-1} (Supplementary Table 3).

Frictional stability, as related to earthquake nucleation, is typically presented by the $(a-b)$ parameter of the rate- and state-friction equation (see Methods for the parameter equation), for which negative values indicate the likelihood of earthquake nucleation[29–31] (Fig. 4a). All tested samples display dominantly stable frictional behaviour ($(a-b)>0$) at shallow depths of 1.5–3.0 km followed by a transition to unstable frictional behaviour at greater depths (Fig. 4a). The unstable behaviour frequently resulted in stick-slip sliding during the experiments for all samples (Supplementary Fig. 6a–d). The sample of the partially dolomitized carbonate vein (Supplementary Fig. 4c) transitioned to unstable behaviour at shallower depths (3 km) and displayed the largest intensity of frictional instability, with large stick-slips by 6 km depth. The granite and rhyolite samples transitioned to fully unstable behaviour at greater depth (4–6 km), consistent with previous experimental behaviour of granite under hydrothermal conditions[8]. The observed transition from stable to unstable slip of the Oklahoma basement samples at depths of 3–6 km corresponds well with the depth distribution of the earthquake hypocentres and major increase in cumulative moment release (Fig. 4b). Our results indicate that extensive

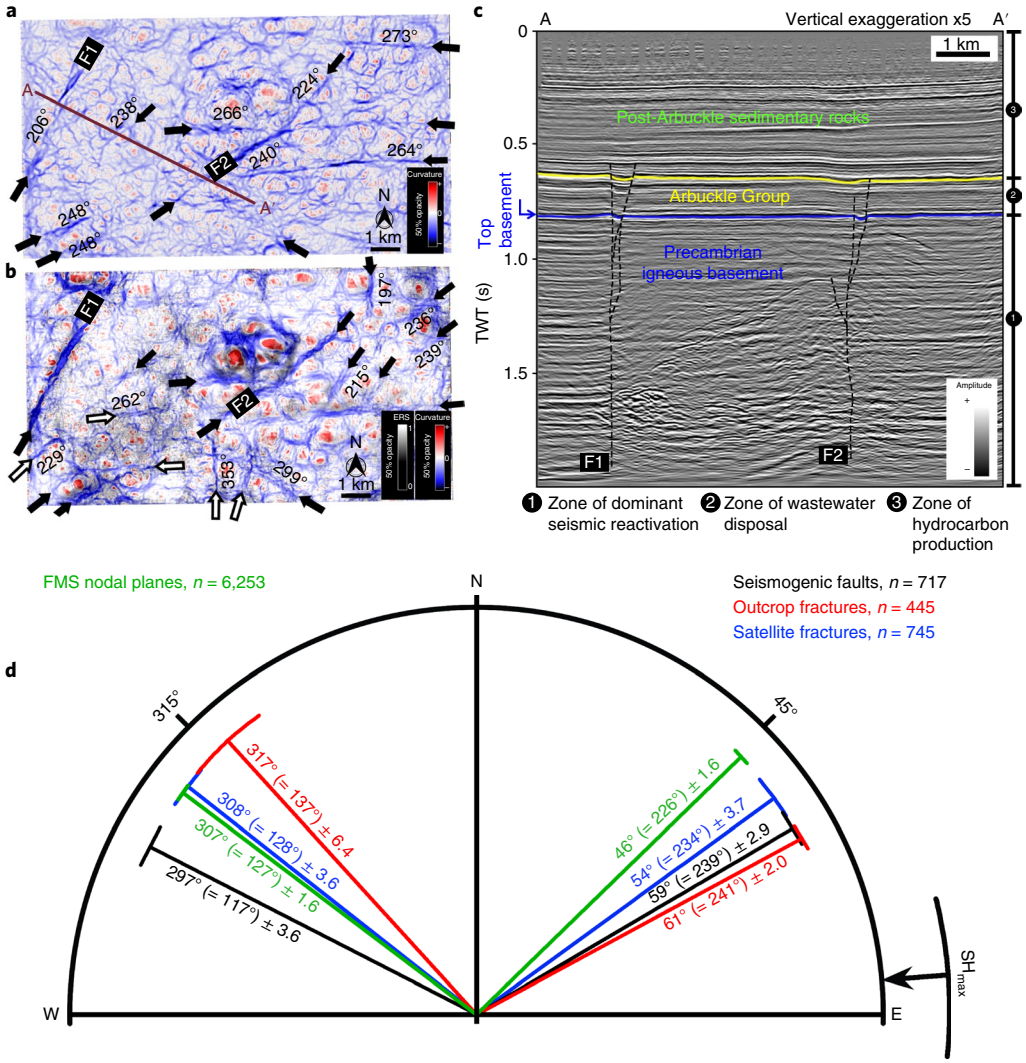

Fig. 3 | Three-dimensional seismic data and structural data compilation. a,**b**, Subsurface structure at location marked in Fig. 1a (white star) based on 3D seismic survey showing time-structure map of top basement (**a**) and top Arbuckle (**b**), co-rendered with curvature and energy-ratio-similarity (ERS) seismic attributes. Black arrows represent lineaments detected in both **a** and **b**; white arrows represent lineaments detected only in **b**. These lineaments are interpreted as fault zones. **c**, Seismic cross-section along A–A′ (in **a**) overlaid with interpretations. F1 and F2 are faults with associated flower structures. Data courtesy of Osage Nation and SpyGlass Energy. **d**, Overlays of frequency-azimuth rose diagrams for satellite-scale fractures, outcrop-scale fractures, seismogenic faults (Fig. 1b; see text) and focal-plane mechanism solution (FMS) nodal planes. Structural trends are described as 'mean trend (=mean trend+180°) ± s.d.'. Arrow represents the estimated maximum horizontal compressive stress (SH_{max}) orientation for Oklahoma[38,42,43].

hydrothermal alteration, observed in many parts of Oklahoma[10–12], could result in seismically unstable fault zone material at shallower depths. Further, we view the stability determinations as a conservative estimate considering the observation of a subhydrostatic gradient in Oklahoma[32] and previous experimental results in granite that show increased instability with lower loading velocities[33], both of which would result in a shallower transition to unstable behaviour.

Oklahoma's susceptibility to seismic reactivation

The results of the present analyses shed light on the basic mechanics that control the recent Oklahoma earthquakes. Our analyses explain why Oklahoma basement faults are susceptible to reactivation by wastewater injection in such a way that has led to the widespread, intense seismicity within the current stress field[2,34]. We discuss here our three main findings and their implications for the observed seismicity.

First, we show a remarkable relationship between the dominant basement fabric and recent earthquake characteristics in Oklahoma. We document these relations via five independent methods (Supplementary Table 1): (1) field mapping of fracture and fault networks (Fig. 2a–d and Supplementary Figs. 1a and 2a,b), (2) satellite-scale mapping of fracture systems (Supplementary Fig. 1b,c), (3) subsurface mapping of fault zones (Fig. 3a–c), (4) delineation of earthquake cluster lineaments (Fig. 1b and Supplementary Fig. 3a) and (5) compilation of nodal planes from earthquake focal-mechanism solutions (Supplementary Fig. 3b). The observations indicate the existence of a tectonic fabric with dominant discontinuity zones within the Precambrian basement that trend northeast–southwest and northwest–southeast (Fig. 3d). These pre-existing faults are weak zones waiting to be reactivated, similar to previously documented reactivation of basement faults in the New Madrid area of the central United States[35]. Further, the reactivation of faults can occur even under unfavourably oriented stresses[36] or after long periods (>2 Gyr) of inactivity[37]. In Oklahoma, the faults trending northeast–southwest and northwest–southeast are favourably oriented relative to the maximum horizontal compressive stress that

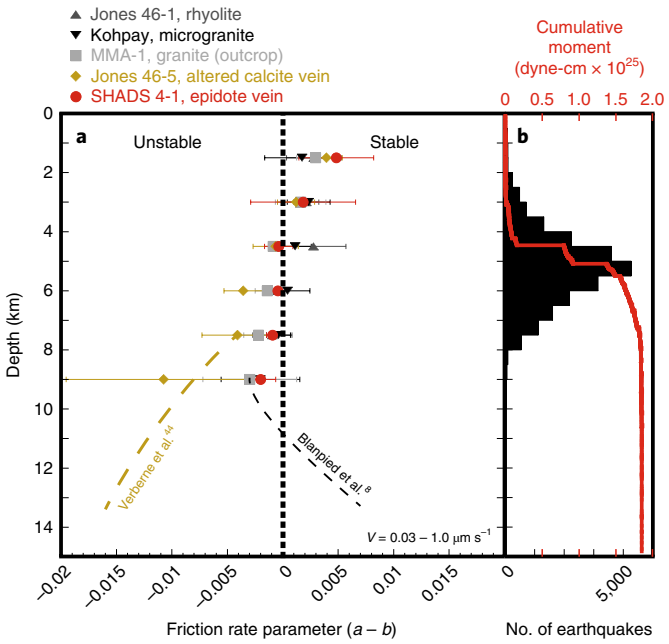

Fig. 4 | Depth distribution of seismic stability and earthquakes in Oklahoma. a, Seismic stability of Oklahoma basement samples as represented by the rate- and state-friction parameter ($a-b$). The symbol shows the average of the velocity steps tested, and the error bars show the range of values for each experimental sample and depth. Gold and black dashed lines represent projection of data for pure calcite[44] and Westerly granite[8], respectively. **b**, Histogram and cumulative moment[45] with depth for the relocated Oklahoma earthquakes (this study) for the period 2010–2017.

strikes ~80°/260° in the midcontinent United States, determined before the recent seismic activity[38]. Therefore, the pre-existing faults documented in the present study are critically stressed for strike-slip motion and are thus expected to be reactivated, even by stress or pore pressure perturbations of 2 MPa and less[39,40].

Second, a crucial observation of the subsurface analysis is that the basement fault zones cut into the Arbuckle Group and shallower units (Fig. 3a–c). This is a direct observation of physical connectivity between the Arbuckle Group, which is the main unit for wastewater disposal in Oklahoma, and underlying basement faults (Fig. 3c). The existence of such fluid migration pathways is an essential component for fast earthquake triggering by wastewater injection. For example, the foreshocks leading up to the 2016 M_w 5.8 Pawnee earthquake (Fig. 1a) were near-instantaneous responses to variations in injection rates at disposal wells within a 20 km radius of the mainshock[5,40].

Third, our rock-mechanics analysis of Oklahoma basement rocks and hydrothermal alteration products (Supplementary Table 2) shows that these rocks become seismically unstable under in situ depth conditions (temperature, pressure and water saturation) of 3–6 km (Fig. 4a). Thus, fault zones composed of these rocks are likely to nucleate earthquakes, rather than creep, at depths >3 km. This transition to unstable slip well explains the depth distribution of the hypocentres and moments with concentration at 3–6 km depth interval (Fig. 4b) and further explains the relatively small number of earthquakes at the wastewater injection depths of <3 km below the surface[6].

Our analyses provide the essential ingredients for understanding the current induced seismicity by wastewater injection in Oklahoma. We show that Oklahoma is prone to widespread seismicity by reactivation of pre-existing basement structures facilitated by the key properties of these structures. It is suspected that other regions of intense wastewater injection, for example, Texas and South Dakota, which display substantially lower levels of induced earthquakes, lack one or more of the needed ingredients highlighted in this study.

Online content

Any methods, additional references, Nature Research reporting summaries, source data, statements of code and data availability and associated accession codes are available at https://doi.org/10.1038/s41561-019-0440-5.

Received: 29 November 2018; Accepted: 2 August 2019;
Published online: 16 September 2019

References

1. Ellsworth, W. L. Injection-induced earthquakes. *Science* **341**, 1225942 (2013).
2. Keranen, K. M., Weingarten, M., Abers, G. A., Bekins, B. A. & Ge, S. Sharp increase in central Oklahoma seismicity since 2008 induced by massive wastewater injection. *Science* **345**, 448–451 (2014).
3. Walsh, F. R. III & Zoback, M. D. Oklahoma's recent earthquakes and saltwater disposal. *Sci. Adv.* **1**, e1500195 (2015).
4. Schultz, R., Wang, R., Gu, Y. J., Haug, K. & Atkinson, G. A seismological overview of the induced earthquakes in the Duvernay play near Fox Creek, Alberta. *J. Geophys. Res. Solid Earth* **122**, 492–505 (2017).
5. Chen, X. et al. The Pawnee earthquake as a result of the interplay among injection, faults and foreshocks. *Sci. Rep.* **7**, 4945 (2017).
6. Goebel, T. H. W., Weingarten, M., Chen, X., Haffener, J. & Brodsky, E. E. The 2016 M_w 5.1 Fairview, Oklahoma earthquakes: evidence for long-range poroelastic triggering at >40 km from fluid disposal wells. *Earth Planet. Sci. Lett.* **472**, 50–61 (2017).
7. McGarr, A. & Barbour, A. J. Wastewater disposal and the earthquake sequences during 2016 near Fairview, Pawnee, and Cushing, Oklahoma. *Geophys. Res. Lett.* **44**, 9330–9336 (2017).
8. Blanpied, M. L., Lockner, D. A. & Byerlee, J. D. Fault stability inferred from granite sliding experiments at hydrothermal conditions. *Geophys. Res. Lett.* **18**, 609–612 (1991).
9. Bickford, M. E., Van Schmus, W. R., Karlstrom, K. E., Mueller, P. A. & Kamenov, G. D. Mesoproterozoic-trans-Laurentian magmatism: a synthesis of continent-wide age distributions, new SIMS U–Pb ages, zircon saturation temperatures, and Hf and Nd isotopic compositions. *Precambrian Res.* **265**, 286–312 (2015).
10. Lidiak, E. G., Denison, R. E. & Stern, R. J. Cambrian (?) Mill Creek diabase dike swarm, eastern Arbuckles: a glimpse of Cambrian rifting in the Southern Oklahoma Aulacogen. *Okla. Geol. Surv. Guideb.* **38**, 105–122 (2014).
11. Denison, R. E. *Basement Rocks in Northeastern Oklahoma* Circular 84 (Oklahoma Geological Survey, The University of Oklahoma Printing Services, 1981).
12. Denison, R. E., Lidiak, E. G., Bickford, M. E. & Kisvarsanyi, E. B. *Geology and Geochronology of Precambrian Rocks in the Central Interior Region of the United States* Professional Paper 1241-C (US Geological Survey, 1984).
13. Shah, A. K. & Keller, G. R. Geologic influence on induced seismicity: constraints from potential field data in Oklahoma. *Geophys. Res. Lett.* **44**, 152–161 (2017).
14. Cannon, W. F. Closing of the Midcontinent Rift—a far-field effect of Grenvillian compression. *Geology* **22**, 155–158 (1994).
15. Brewer, J. A., Good, R., Oliver, J. E., Brown, L. D. & Kaufman, S. COCORP profiling across the Southern Oklahoma aulacogen: overthrusting of the Wichita Mountains and compression within the Anadarko Basin. *Geology* **11**, 109–114 (1983).
16. Powers, S. Age of the folding of the Oklahoma mountains—the Ouachita, Arbuckle, and Wichita mountains of Oklahoma and the Llano-Burnet and Marathon uplifts of Texas. *Geol. Soc. Am. Bull.* **39**, 1031–1071 (1928).
17. Keller, G. R. & Stephenson, R. A. The Southern Oklahoma and Dniepr-Donets aulacogens: a comparative analysis. *Geol. Soc. Am. Mem.* **200**, 127–143 (2007).
18. Denison, R. E. Significance of air-photograph linears in the basement rocks of the Arbuckle Mountains. In *Structural Styles in the Southern Midcontinent, 1992 Symposium* (ed. Johnson, K. S.) 119–131 (Oklahoma Geological Survey, 1995).
19. Barton, N. & Choubey, V. The shear strength of rock joints in theory and practice. *Rock. Mech.* **10**, 1–54 (1977).
20. Martin, C. D. & Stimpson, B. The effect of sample disturbance on laboratory properties of Lac du Bonnet granite. *Can. Geotech. J.* **31**, 692–702 (1994).
21. Segall, P. & Pollard, D. D. Nucleation and growth of strike slip faults in granite. *J. Geophys. Res. Solid Earth* **88**, 555–568 (1983).

22. Barton, C. A. & Zoback, M. D. Self-similar distribution and properties of macroscopic fractures at depth in crystalline rock in the Cajon Pass scientific drill hole. *J. Geophys. Res.* **97**, 5181–5200 (1992).
23. Sagy, A., Reches, Z. E. & Roman, I. Dynamic fracturing: field and experimental observations. *J. Struct. Geol.* **23**, 1223–1239 (2001).
24. Fielding, E. J., Sangha, S. S., Bekaert, D. P., Samsonov, S. V. & Chang, J. C. Surface deformation of north-central Oklahoma related to the 2016 M_w 5.8 Pawnee earthquake from SAR interferometry time series. *Seismol. Res. Lett.* **88**, 971–982 (2017).
25. Elebiju, O. O., Matson, S., Keller, G. R. & Marfurt, K. J. Integrated geophysical studies of the basement structures, the Mississippi chert, and the Arbuckle Group of Osage County region, Oklahoma. *Am. Assoc. Pet. Geol. Bull.* **95**, 371–393 (2011).
26. McGarr, A. & Barbour, A. J. Injection-induced moment release can also be aseismic. *Geophys. Res. Lett.* **45**, 5344–5351 (2018).
27. Moore, D. E. & Lockner, D. A. Frictional strengths of talc-serpentine and talc-quartz mixtures. *J. Geophys. Res. Solid Earth* **116**, B01403 (2011).
28. Harrison, W. E., Luza, K. V., Prater, M. L., Cheung, P. K. & Ruscetta, C. A. *Geothermal Resource Assessment in Oklahoma* No. DOE/ID/12079-71-Vol. 1/ESL-98-Vol. 1/CONF-820491 1–12 (Earth Science Laboratory, University of Utah Research Institute, 1982).
29. Dieterich, J. H. Modeling of rock friction 1. Experimental results and constitutive equations. *J. Geophys. Res.* **84**, 2161–2168 (1979).
30. Marone, C. Laboratory-derived friction laws and their application to seismic faulting. *Annu. Rev. Earth Planet. Sci.* **26**, 643–696 (1998).
31. Ikari, M. J., Marone, C. & Saffer, D. M. On the relation between fault strength and frictional stability. *Geology* **39**, 83–86 (2011).
32. Nelson, P. H., Gianoutsos, N. J. & Drake, R. M. Underpressure in Mesozoic and Paleozoic rock units in the Midcontinent of the United States. *Am. Assoc. Pet. Geol. Bull.* **99**, 1861–1892 (2015).
33. Blanpied, M. L., Tullis, T. E. & Weeks, J. D. Effects of slip, slip rate, and shear heating on the friction of granite. *J. Geophys. Res.* **103**, 489–511 (1998).
34. Keranen, K. M., Savage, H. M., Abers, G. A. & Cochran, E. S. Potentially induced earthquakes in Oklahoma, USA: links between wastewater injection and the 2011 M_w 5.7 earthquake sequence. *Geology* **41**, 699–702 (2013).
35. Hurd, O. & Zoback, M. D. Regional stress orientations and slip compatibility of earthquake focal planes in the New Madrid seismic zone. *Seismol. Res. Lett.* **83**, 672–679 (2012).
36. Reches, Z. Analysis of faulting in three-dimensional strain field. *Tectonophysics* **47**, 109–129 (1978).
37. Heesakkers, V., Murphy, S., Lockner, D. A. & Reches, Z. Earthquake rupture at focal depth, part II: mechanics of the 2004 *M* 2.2 earthquake along the Pretorius Fault, TauTona Mine, South Africa. *Pure Appl. Geophys.* **168**, 2427–2449 (2011).
38. Zoback, M. D. & Zoback, M. L. in *Neotectonics of North America* (eds Slemmons, D. B., et al.) 339–366 (Geological Society of America, 1991).
39. Walsh, F. R. III & Zoback, M. D. Probabilistic assessment of potential fault slip related to injection-induced earthquakes: application to north-central Oklahoma, USA. *Geology* **44**, 991–994 (2016).
40. Barbour, A. J., Norbeck, J. H. & Rubinstein, J. L. The effects of varying injection rates in Osage County, Oklahoma, on the 2016 M_w 5.8 Pawnee earthquake. *Seismol. Res. Lett.* **88**, 1040–1053 (2017).
41. Marsh, S. & Holland, A. *Comprehensive Fault Database and Interpretive Fault Map of Oklahoma* Open-File Report OF2-2016 (Oklahoma Geological Survey, 2016).
42. Qi, W. *Stress Analysis of Recent Earthquakes in Oklahoma*. MSc thesis, University of Oklahoma (2016).
43. Alt, R. C. & Zoback, M. D. In situ stress and active faulting in Oklahoma. *Bull. Seismol. Soc. Am.* **107**, 216–228 (2016).
44. Verberne, B. A., Niemeijer, A. R., De Bresser, J. H. P. & Spiers, C. J. Mechanical behavior and microstructure of simulated calcite fault gouge sheared at 20–600 °C: implications for natural faults in limestones. *J. Geophys. Res. Solid Earth* **120**, 8169–8196 (2015).
45. Kanamori, H. Magnitude scale and quantification of earthquakes. *Tectonophysics* **93**, 185–199 (1983).

Acknowledgements

We acknowledge the USGS Induced Seismicity Project for providing financial support and laboratory expertise/time to conduct the experiments presented in this manuscript. We thank N. Beeler and A. Barbour for their helpful reviews. We thank Osage Nation and SpyGlass Energy, LLC, for providing the seismic data used in this study. We also thank the Oklahoma Geological Survey for providing earthquake and focal mechanism data.

Author contributions

F.K., D.A.L., Z.R. and B.M.C. wrote the manuscript. F.K. and C.S.J. performed satellite fracture mapping. F.K., C.S.J., Z.R. and B.M.C. completed the fieldwork. J.C.C. assisted with earthquake relocation and epicentre-cluster lineament mapping. F.K. and K.J.M. completed the 3D seismic analysis. C.B.M., D.A.L., Z.R. and B.M.C. designed, performed, and analysed the friction experiments.

Competing interests

The authors declare no competing interests.

Additional information

Supplementary information is available for this paper at https://doi.org/10.1038/s41561-019-0440-5.

Reprints and permissions information is available at www.nature.com/reprints.

Correspondence and requests for materials should be addressed to B.M.C.

Methods

Seismic attributes. The seismic survey used in this study includes a post-stack time-migrated 3D seismic volume with bin size of 20 × 20 m and an estimated limit of vertical resolution of 25 m. We used curvature and coherence seismic attributes[46] to better resolve subsurface structures and basement fault zones along the top-Arbuckle Group surface map (the preferred unit for wastewater injection)[47] and the top-basement surface map (zone of most frequent seismicity)[48]. Structural deformation such as flexural and stepped block faulting are revealed by the positive and negative curvature seismic attributes, where the most positive curvature ($k1$) highlights up-warped/up-thrown zones and the most negative curvature ($k2$) highlights down-warped/down-thrown areas along the seismic reflectors associated with the mapped surfaces. These curvature attributes are sensitive to fault zones characterized by small vertical offsets and subtle structural flexures often typical of strike-slip faults. The edge-detection energy ratio similarity (coherence) attribute computes the ratio of the coherent energy of the data to the total energy of the traces within an analyses window. The energy ratio similarity attribute is sensitive to zones of discontinuity along a reflector, thus revealing fault damage zones as lineaments of low energy relative to the surrounding intact rocks of higher energy (Fig. 3a,b). In this study, we computed the volumetric seismic attributes in the Attribute-Assisted Seismic Processing and Interpretation (AASPI) software application from University of Oklahoma, then extracted and co-rendered the generated attributes in a PETREL software application.

Earthquake relocation. We obtained 10,879 earthquake events of $M_w \geq 0$ for the period 2010–2017 from the Oklahoma Geological Survey earthquake catalogue (http://www.ou.edu/ogs/research/earthquakes/catalogs) and relocated the events by using HypoDD and phase picking for 1D velocity modelling following the methods of Fielding et al.[24] and Waldhauser and Ellsworth[49]. About 2–4% of the events in the Oklahoma Geological Survey earthquake catalogue occurred in the period preceding the uptick in seismicity in Oklahoma (1882–2009). Since there are no phase picks in these old data, we could not include pre-2010 data in our relocated catalogue.

Experimental samples. We measured the mechanical behaviour of five basement rock samples obtained in Oklahoma (Supplementary Table 2). Four of the samples were derived from core material collected in three wells that penetrated the top of the igneous basement in the north-central region of the state (Supplementary Fig. 4). The Jones 46 and SHADS 4 samples are from the Washington Volcanic Group, whereas the Kohpay sample is from the Osage County Microgranite[12]. The MMA-1 sample is an outcrop sample from a Martin Marietta Aggregates quarry in south-central Oklahoma and is derived from the Troy Granite ('Q' in Fig. 1d). All borehole core samples were collected at the Oklahoma Petroleum Information Center (OPIC) core repository in Norman, Oklahoma. Samples were collected as intact core or rubble. All samples were pulverized in a disk mill until all material passed through a 150 µm sieve. The resulting gouge was then wetted to make a paste that formed a 1 mm experimental gouge layer.

Friction tests. The experiments were performed in a standard triaxial apparatus (Supplementary Fig. 5a). The 1 mm gouge layer was sandwiched within the sawcut of 19-mm-diameter granite forcing blocks. The sawcut, inclined at 30° (Supplementary Fig. 5b), was roughened with 100 grit abrasive to ensure distributed deformation within the gouge layer[27]. The top forcing block had a hole drilled through it to allow pore pressure communication with the gouge layer. Conditions for the experiments were chosen to represent depth conditions (confining pressure, pore pressure and temperature) within the crust (Supplementary Table 3). Temperature calculations were based on a 23 °C km^{-1} (ref. [28]), which is a reasonable approximation for the Precambrian crust of the midcontinent. Pore pressure was set to be hydrostatic, 10 MPa km^{-1}, and effective confining pressure was set to be 17.5 MPa km^{-1}. All samples were saturated with a solution of deionized water that was allowed to equilibrate with granite rubble for 24 h. All experimental conditions are shown in Supplementary Table 3.

Samples were jacketed in a lead jacket for isolation from confining fluid. A greased Teflon shim was placed between the piston and the sample assembly to allow for lateral slip of the lower driving block during shear. A shear strength correction, due to the stretching of the lead jacket, was applied to the measured shear stress. Shear and normal stresses were also corrected for the reduction in contact area as the two sample halves slide past each other. Axial load was measured with an external load cell. Confining and pore pressures were measured at a rate of 1 Hz. Shear and normal stress resolved on the fault surface were computed in real time from the axial stress, confining pressure and axial shortening. Confining pressure was modified in real time to maintain a constant resolved normal stress on the experimental fault plane. Axial stress, confining pressure and pore pressure have accuracies of at least 0.03 MPa. Sample strength is reported as the coefficient of friction. Within a single experiment, changes in the coefficient of friction have a precision of ±0.001. After correcting for true contact area and jacket strength, the determined coefficient of friction has an accuracy of ±0.01.

Samples were sheared to a total of ~4.0 mm axial shortening. Axial shortening rates were stepped in the following sequence to determine the dependence of friction on shear velocity: 1.0–0.3–0.1–0.03–0.1–0.3–1–0.5 µm s^{-1}. Due to the 30° sawcut, slip and slip rate on the inclined fault surfaces were 15% higher than the corresponding axial values.

The friction rate parameter was determined by manually measuring the change in friction ($\Delta\mu$) due to a velocity step from a detrended friction-displacement curve. Detrending was necessary to remove long-term strain hardening trends. The measured $\Delta\mu$ values were then used to calculate the friction rate parameter ($a-b$) via:

$$(a-b) = (\Delta\mu)/\ln(V/V_0)$$

where V_0 is the velocity before the velocity step and V is the velocity following the step[29,50]. Where samples were failing by stick-slip, $\Delta\mu$ was measured between the average friction before/after the velocity step.

Data availability

All data and materials that support the findings of this study can be made available, in some form, to any researcher for purposes of reproducing or extending the analysis upon request to the corresponding author. The 3D seismic data from Osage County are publicly available through Osage Nation. Oklahoma Geological Survey data products can be found at www.ou.edu/ogs. Field mapping data can be provided upon request by contacting the corresponding author. Laboratory data appearing in Supplementary Figs. 4 and 6 acquired during experiments at the US Geological Survey in Menlo Park, California, and the friction data used in this study can be obtained from https://doi.org/10.5066/P9AJWOZD.

References

46. Chopra, S. & Marfurt, K. J. *Seismic Attributes for Prospect Identification and Reservoir Characterization* (Society of Exploration Geophysicists, 2007).
47. Kroll, K. A., Cochran, E. S. & Murray, K. E. Poroelastic properties of the Arbuckle Group in Oklahoma derived from well fluid level response to the 3 September 2016 M_w 5.8 Pawnee and 7 November 2016 M_w 5.0 Cushing earthquakes. *Seismol. Res. Lett.* **88**, 963–970 (2017).
48. Schoenball, M. & Ellsworth, W. L. Waveform-relocated earthquake catalog for Oklahoma and southern Kansas illuminates the regional fault network. *Seismol. Res. Lett.* **88**, 1252–1258 (2017).
49. Waldhauser, F. & Ellsworth, W. L. A double-difference earthquake location algorithm: method and application to the northern Hayward fault. *Calif. Bull. Seismol. Soc. Am.* **90**, 1353–1368 (2000).
50. Ruina, A. Slip instability and state variable friction laws. *J. Geophys. Res.* **88**, 10359–10370 (1983).